

# Thermochemical and Kinetic Analysis on the Reactions of O<sub>2</sub> with Products from OH Addition to Isobutene, 2-Hydroxy-1,1-dimethylethyl, and 2-Hydroxy-2-methylpropyl Radicals: HO<sub>2</sub> Formation from Oxidation of Neopentane, Part II

Hongyan Sun,<sup>†</sup> Joseph W. Bozzelli,<sup>\*,‡</sup> and Chung K. Law<sup>†</sup>

Department of Mechanical and Aerospace Engineering, Princeton University, Princeton, New Jersey 08544,  
Department of Chemistry and Environmental Science, New Jersey Institute of Technology,  
Newark, New Jersey 07102

Received: January 4, 2007; In Final Form: March 16, 2007

Unimolecular dissociation of a neopentyl radical to isobutene and methyl radical is competitive with the neopentyl association with O<sub>2</sub>(<sup>3</sup>Σ<sub>g</sub><sup>-</sup>) in thermal oxidative systems. Furthermore, both isobutene and the OH radical are important primary products from the reactions of neopentyl with O<sub>2</sub>. Consequently, the reactions of O<sub>2</sub> with the 2-hydroxy-1,1-dimethylethyl and 2-hydroxy-2-methylpropyl radicals resulting from the OH addition to isobutene are important to understanding the oxidation of neopentane and other branched hydrocarbons. Reactions that correspond to the association of radical adducts with O<sub>2</sub>(<sup>3</sup>Σ<sub>g</sub><sup>-</sup>) involve chemically activated peroxy intermediates, which can isomerize and react to form one of several products before stabilization. The above reaction systems were analyzed with ab initio and density functional calculations to evaluate the thermochemistry, reaction paths, and kinetics that are important in neopentyl radical oxidation. The stationary points of potential energy surfaces were analyzed based on the enthalpies calculated at the CBS-Q level. The entropies,  $S^{\circ}_{298}$ , and heat capacities,  $C_p(T)$ , ( $0 \leq T/K \leq 1500$ ), from vibration, translation, and external rotation contributions were calculated using statistical mechanics based on the vibrational frequencies and structures obtained from the density functional study. The hindered internal rotor contributions to  $S^{\circ}_{298}$  and  $C_p(T)$  were calculated by solving the Schrödinger equation with free rotor wave functions, and the partition coefficients were treated by direct integration over energy levels of the internal rotation potentials. Enthalpies of formation ( $\Delta H_f^{\circ}_{298}$ ) were determined using isodesmic reaction analysis. The  $\Delta H_f^{\circ}_{298}$  values of (CH<sub>3</sub>)<sub>2</sub>C•CH<sub>2</sub>OH, (CH<sub>3</sub>)<sub>2</sub>C(OO•)CH<sub>2</sub>OH, (CH<sub>3</sub>)<sub>2</sub>C(OH)C•H<sub>2</sub>, and (CH<sub>3</sub>)<sub>2</sub>C(OH)CH<sub>2</sub>OO• radicals were determined to be -23.3, -62.2, -24.2, and -61.8 kcal mol<sup>-1</sup>, respectively. Elementary rate constants were calculated from canonical transition state theory, and pressure-dependent rate constants for multichannel reaction systems were calculated as functions of pressure and temperature using multifrequency quantum Rice–Ramsperger–Kassel (QRRK) analysis for  $k(E)$  and a master equation for pressure falloff. Kinetic parameters for intermediate and product formation channels of the above reaction systems are presented as functions of temperature and pressure.

## Introduction

Low-temperature hydrocarbon oxidation proceeds via reactions involving alkyl and alkylperoxy radicals that play a critical role in such practical combustion systems as the auto-ignition in homogeneous charge compression ignition (HCCI) engines and the pre-ignition associated with engine knock. Compared to most alkane oxidation systems, the neopentane moiety has unique features that facilitate a simpler interpretation of experimental results.<sup>1</sup> However, the overall interpretation of early time products from the oxidation of neopentyl radical is complex because of the competition from the oxidation products of isobutene and a methyl radical, which are produced from the competing β-scission of the neopentyl radical. Furthermore, both isobutene and OH radical are important primary products from the reactions of neopentyl with O<sub>2</sub>(<sup>3</sup>Σ<sub>g</sub><sup>-</sup>). Consequently,

the reactions of O<sub>2</sub>(<sup>3</sup>Σ<sub>g</sub><sup>-</sup>) with the radical adducts resulting from the OH addition to isobutene are essential to the understanding of the oxidation of neopentane and other branched hydrocarbons.

Recently, Taatjes et al.<sup>2,3</sup> measured the time-resolved production of HO<sub>2</sub> and OH in the pulsed-photolytic Cl-initiated oxidation of neopentane between 573 and 750 K and observed significant HO<sub>2</sub> formation above 623 K. Furthermore, they also found that the formation of HO<sub>2</sub> increases with increasing temperature and that the overall amount of HO<sub>2</sub> produced increases with increasing O<sub>2</sub> concentration at 673 K. The ad hoc kinetic model by Taatjes et al.<sup>2,3</sup> predicted well for their experimental OH formation versus time at 673 K, although it failed to predict the increase in HO<sub>2</sub> at higher O<sub>2</sub> concentration. Hence they indicated that the agreement could be improved by including the complete chemistry of the initial and secondary peroxy radical systems in their model.<sup>2,3</sup> It is noted that these experimental data on the OH and HO<sub>2</sub> profiles in flames from neopentane combustion are also valuable for the comparison and validation of kinetic models.

\* Corresponding author. E-mail: Bozzelli@njit.edu.

<sup>†</sup> Department of Mechanical and Aerospace Engineering, Princeton University.

<sup>‡</sup> Department of Chemistry and Environmental Science, New Jersey Institute of Technology.

The neopentyl radical plus oxygen system has a number of product channels as illustrated in our ab initio and density functional studies<sup>1</sup> and is in competition with the  $\beta$ -scission of the neopentyl radical to isobutene plus methyl radical. The important initial products in the neopentyl radical reaction with O<sub>2</sub> are: neopentyl-peroxy, OH and CH<sub>3</sub> radicals, and isobutene. The addition of an OH radical to the isobutene at the CD/H<sub>2</sub> and CD/C<sub>2</sub> carbon atoms (CD represents carbon double bond group) forms two new radical products, 2-hydroxy-1,1-dimethylethyl and 2-hydroxy-2-methylpropyl radicals, which undergo further oxidation by reacting with O<sub>2</sub>. The oxidation reactions of these products resulting from hydroxyl or methyl radical addition to the isobutene intermediate need to be studied further, as they are important to model the formation of intermediates and end products in the oxidative or thermal reactions of neopentane.

The reactions of O<sub>2</sub> with the two adducts from OH addition to isobutene were previously estimated by THERM<sup>5</sup> and PM3<sup>6,7</sup> methods and other estimation techniques by Chen and Bozzelli<sup>4</sup> as a submechanism of tertiary butyl radical oxidation.<sup>4</sup> In the present study, the thermochemistry and the stationary points on the potential energy surfaces of 2-hydroxy-1,1-dimethylethyl and 2-hydroxy-2-methylpropyl radicals with O<sub>2</sub>(<sup>3</sup> $\Sigma_g^-$ ) were characterized by using ab initio and density functional calculations, and new important reaction channels were found. Thermochemical and kinetic parameters along with the reaction paths were determined for these R• + O<sub>2</sub> reactions, which are important in neopentyl and similar branched hydrocarbon radical oxidation.

## Calculation Methods

The geometries of reactants, intermediates, transition states, and products in the two reaction systems were calculated at the B3LYP/6-31G(d,p)<sup>8</sup> level using the Gaussian 98/Gaussian 03 programs.<sup>9,10</sup> The optimized structure parameters were then used to obtain total electronic energies at the B3LYP/6-311++G-(3df,2p)<sup>8</sup> and CBS-Q<sup>11</sup> single-point levels of calculation. These data were used along with isodesmic reactions to determine the standard enthalpies of formation at 298 K. The CBS-Q enthalpies based on the B3LYP/6-31G(d,p) optimized geometries are referred to as CBSQ//B3LYP in our study. The CBSQ//B3LYP method for the estimation of the  $\Delta H_f^\circ_{298}$  values on hydrocarbons, oxy-substituted hydrocarbons, and the corresponding radicals has been evaluated in our previous studies,<sup>1,12,13</sup> where it shows good accuracy and precision with accepted literature values. The discrepancy between activation energies calculated at the CBSQ//B3LYP level with the values at the CBS-QB3 level is within 1 kcal mol<sup>-1</sup>. Contributions from translation, vibration, external rotation, and electronic motion to entropies and heat capacities were calculated by statistical mechanics based on the vibration frequencies and moments of inertia from the DFT optimized structures. The torsion frequencies were omitted in the calculation of  $S^\circ_{298}$  and  $C_p(T)$ ; their contributions were determined by summation over the energy levels obtained by direct diagonalization of the Hamiltonian matrix of hindered internal rotations represented by the truncated Fourier series as  $a_0 + \sum a_i \cos(i\varphi) + \sum b_i \sin(i\varphi)$  with  $\varphi \leq 8$ .<sup>14,15</sup> The  $H_f^\circ_{298}$  values for reactants, intermediates, and products were calculated using the total energies from ab initio and DFT calculations and isodesmic reactions with group balance when possible. The  $\Delta H_f^\circ_{298}$  values of transition state structures were calculated by using the  $\Delta H_f^\circ_{298}$  of stable radical adducts from isodesmic reaction analysis plus the difference of total energies between transition states and radical adducts.

Unimolecular dissociation and isomerization of the chemically activated and stabilized adducts, resulting from addition reactions, were analyzed by first constructing potential energy diagrams for the reaction systems. The DFT and ab initio calculations were then used to determine the transition state structures and activation energies for the isomerization,  $\beta$ -scission, and dissociation reactions. The enthalpies and entropies were treated with conventional transition state theory to calculate the Arrhenius pre-exponential factors and activation energies as functions of temperature. The data were then fitted by a nonlinear least-squares method to the modified Arrhenius equation,  $k_\infty = AT^n \exp(-E_a/RT)$  over the temperature range of 300–2000 K.

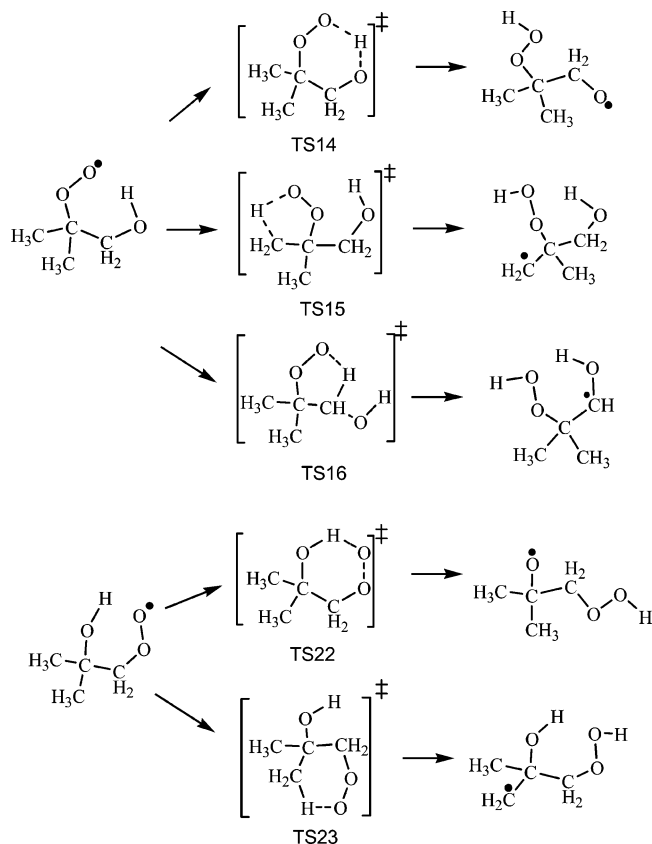
Kinetic parameters for the bimolecular chemical activation reactions and the subsequent unimolecular thermal dissociation reactions to adducts and product sets were calculated by using a multifrequency quantum Rice–Ramsperger–Kassel (QRRK) analysis for  $k(E)$ ,<sup>16</sup> with the steady-state assumption of the energized adduct(s) in combination with a master equation analysis for the pressure falloff.<sup>17</sup> The QRRK code utilizes a reduced set of three vibration frequencies that accurately reproduce the molecular (adduct) heat capacity data.<sup>5,18</sup> Molecular density-of-state functions were constructed through direct convolution of single-frequency density functions on a 10 cm<sup>-1</sup> grid. The functions corresponding to each reduced frequency are explicitly convolved into a relative density-of-states ( $\rho(E)$ ), which is normalized by the partition function ( $Q$ ). The inclusion of one external rotation, corresponding to the symmetric top, is incorporated into the calculations by convolving the vibrational density function with the proper rotational density function.

The collisional deactivation of the energized adduct was calculated using a master equation analysis by Sheng et al.<sup>17</sup> The  $(\Delta E)^\circ_{\text{down}}$  of 570 cal mol<sup>-1</sup> for the collisional deactivation with helium as the third body was used in the master equation analysis. A 0.5 kcal energy interval was used in calculation of rate constants as functions of temperature and pressure for the chemical activation and dissociation reactions. Lennard-Jones parameters,  $\sigma$  (Å) and  $\epsilon/\kappa$  (K), were obtained from tabulations<sup>19</sup> and from an estimation method based on molar volumes and compressibility.<sup>20</sup>

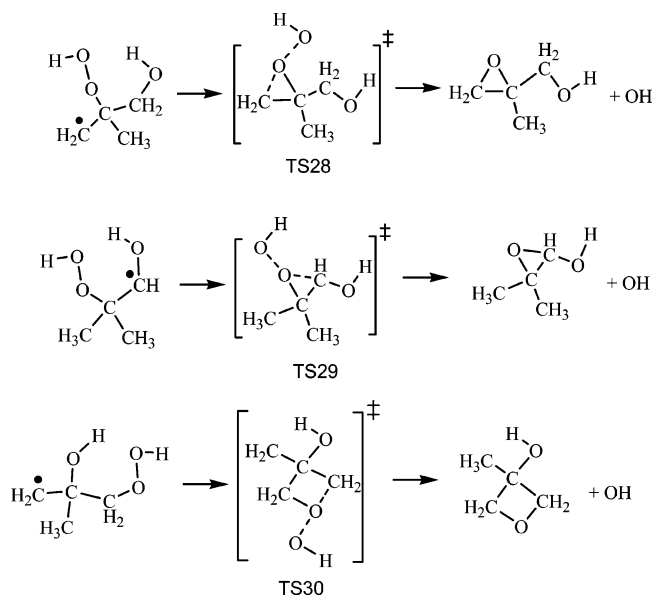
## Results and Discussion

**1. Geometries of Reactants, Intermediate Radicals, and Transition States.** The geometry optimization for the reactants, transition states, adducts, and products in the two isobutene–OH adduct oxidation systems was performed at the B3LYP/6-31G(d,p) level. The optimized structural parameters of 34 species are provided in Supporting Information Table S1. The corresponding unscaled vibration frequencies and moments of inertia are provided in Table S2. The transition states on several types of reactions in the two oxidation systems were identified as follows:

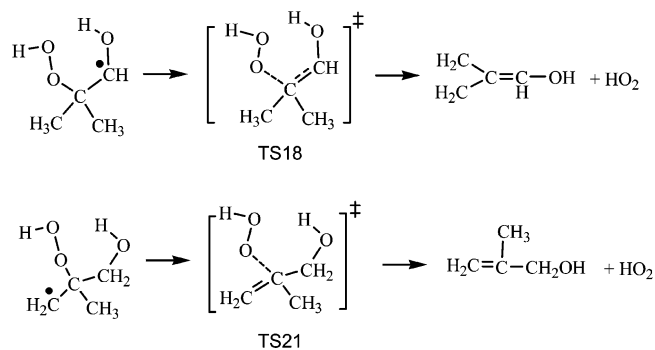
*Hydrogen Atom Transfer: Peroxy Radical Isomerization.* This class of reactions represents intramolecular, endothermic transfer of an H atom from the OH or CH<sub>3</sub> group to the peroxy–oxygen radical site via a five- or six-member ring transition state (includes the H atom). In these transition states, the cleaving O–H bond stretches to 1.35–1.36 Å from 0.96 Å, and the cleaving C–H bond stretches to 1.34–1.42 Å from 1.09 Å, with the forming OO–H bond length of 1.08–1.25 Å. The ROO–H bond length formed in radical intermediates or products is 0.97 Å.



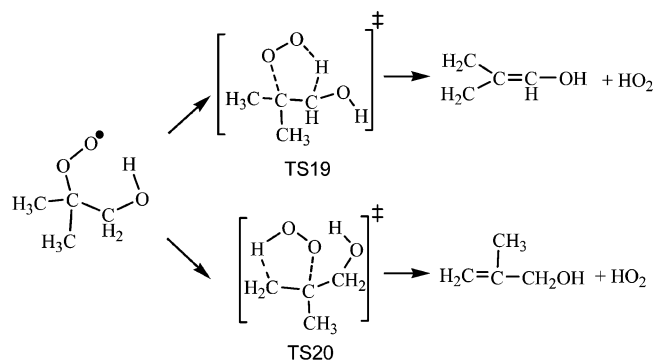
**Epoxide Formation.** In these reactions, the alkyl carbon radical ( $-\text{C}\cdot\text{H}_2$ , or  $-\text{C}\cdot\text{HOH}$  group) attack the oxygen bonded to the carbon atom of the hydroperoxide to form a three- or four-member ring transition state while the weak  $\text{RO}-\text{OH}$  peroxide bond is cleaving. The cleaving  $\text{O}-\text{O}$  bond length is 1.67–1.74 Å, with the forming  $\text{C}-\text{O}$  bond length of 1.92–1.99 Å.



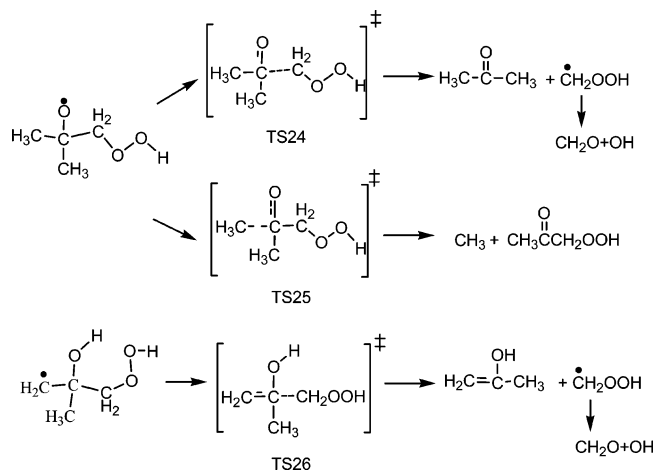
**$\text{HO}_2$  Elimination (via  $\beta$ -Scission).** This reaction type represents the elimination ( $\beta$ -scission) of  $\text{HO}_2$  from a hydroperoxide alkyl radical with olefin formation in the carbon backbone. The cleaving  $\text{C}-\text{O}$  bond length is 1.94–1.99 Å, the forming  $\text{O}-\text{OH}$  bond decreases from 1.46 Å to 1.40–1.42 Å, and the forming  $\text{C}=\text{C}$  bond length is 1.38–1.39 Å in the saddle-point transition state structures.



**Concerted 5-Center  $\text{HO}_2$  Elimination.** This class of reactions represents a concerted elimination of the  $\text{HO}_2$  radical from its alkyl peroxy parent to form an olefin. The  $\text{C}-\text{C}$  bond in the cyclic transition state structure (backbone) assumes a near-planar structure with the cleaving  $\text{C}-\text{O}$  and  $\text{C}-\text{H}$  bonds near perpendicular to the plane ( $\text{HO}_2$  is perpendicular to the forming  $\text{sp}^2$  carbon structure). The  $\text{C}-\text{H}$  and  $\text{C}-\text{O}$  bonds elongate, while the  $\text{O}-\text{O}$  bond length decreases. The saddle-point  $\text{C}-\text{O}$  and  $\text{C}-\text{H}$  bond lengths are 2.28–2.31 Å and 1.340–1.36 Å, respectively, and the forming  $\text{C}=\text{C}$  and  $\text{O}-\text{H}$  bond lengths are 1.39–1.51 Å and 1.28 Å.



**Alkyl Group Elimination.** This class of reactions represents alkyl group or oxy-alkyl group elimination with simultaneous formation of an olefin, with the olefin carbons in a near planar structure. For the  $\beta$ -scission of methyl group in TS25, the  $\text{C}-\text{C}$  bond length stretches from 1.58 to 2.17 Å and forms a  $\text{C}=\text{O}$  bond with transition length of 1.25 Å. In reactions of TS24 and



TS26, the cleaving  $\text{C}-\text{C}$  bond is stretched to 2.06–2.21 Å in length, and the forming  $\text{C}=\text{O}$  and  $\text{C}=\text{C}$  bonds retain 1.26 Å

TABLE 1: Calculated  $\Delta H_f^\circ$  Values by Isodesmic Reaction Analysis<sup>a</sup>

reaction series	B3LYP/6-31G(d,p)		B3LYP/6-311++G(3df,2p)		CBSQ//B3LYP/6-31G(d,p)	
	$\Delta H_{\text{rxn}}^\circ$	$\Delta H_f^\circ$	$\Delta H_{\text{rxn}}^\circ$	$\Delta H_f^\circ$	$\Delta H_{\text{rxn}}^\circ$	$\Delta H_f^\circ$
C <sub>2</sub> C•COH + CH <sub>4</sub> → C•C(OH)C + C <sub>2</sub> H <sub>6</sub>	6.62	-23.92	5.91	-23.21	5.91	-23.21
C <sub>2</sub> C•COH + CH <sub>4</sub> → C•COH + C <sub>3</sub> H <sub>8</sub>	11.37	-24.20	9.64	-22.47	10.53	-23.36
				recommended value:		-23.3
C <sub>2</sub> C(OO•)COH + C <sub>3</sub> H <sub>8</sub> → C <sub>3</sub> CCOO• + CCOH	6.98	-65.69	5.05	-63.76	3.59	-62.30
C <sub>2</sub> C(OO•)COH + C <sub>2</sub> H <sub>6</sub> → CCOO• + C <sub>3</sub> COH	1.36	-62.64	-0.91	-60.37	0.72	-62.00
				recommended value:		-62.2
C <sub>2</sub> •C(OOH)COH + C <sub>2</sub> H <sub>6</sub> → C•COOH + C <sub>3</sub> COH	2.00	-45.52	-0.42	-43.10	2.13	-45.65
C <sub>2</sub> •C(OOH)COH + C <sub>3</sub> H <sub>8</sub> → C <sub>3</sub> •CCOOH + CCOH	7.60	-48.14	5.48	-46.01	5.12	-45.66
				recommended value:		-45.7
C <sub>2</sub> C(OOH)C•OH + CH <sub>4</sub> → C <sub>2</sub> COOH + CC•OH	6.13	-50.54	3.71	-48.12	4.68	-49.09
C <sub>2</sub> C(OOH)C•OH + C <sub>2</sub> H <sub>6</sub> → C <sub>2</sub> COOH + C•C(OH)C	9.27	-52.97	6.51	-50.21	4.84	-48.54
				recommended value:		-48.8
C <sub>2</sub> C(OH)C• + C <sub>2</sub> H <sub>6</sub> → C <sub>3</sub> COH + C <sub>2</sub> H <sub>5</sub>	-0.80	-24.88	-1.11	-24.57	-1.56	-24.12
C <sub>2</sub> C(OH)C• + C <sub>3</sub> H <sub>8</sub> → C <sub>3</sub> CC + C•COH	6.19	-27.05	4.79	-25.65	3.45	-24.31
				recommended value:		-24.2
C <sub>2</sub> C(OH)COO• + CH <sub>4</sub> → CH <sub>3</sub> OO• + C <sub>3</sub> COH	6.76	-61.44	4.48	-59.16	6.83	-61.51
C <sub>2</sub> C(OH)COO• + C <sub>2</sub> H <sub>6</sub> → CCOO• + C <sub>3</sub> COH	1.36	-62.64	-0.91	-60.37	0.72	-62.00
				recommended value:		-61.8
C <sub>2</sub> C(O•)COOH + C <sub>2</sub> H <sub>6</sub> → C <sub>3</sub> CO• + CCOOH	-0.96	-41.64	-2.11	-40.49	-1.38	-41.22
C <sub>2</sub> C(O•)COOH + C <sub>3</sub> H <sub>8</sub> → C <sub>3</sub> CO• + CCOOH	-0.65	-42.24	-1.63	-41.26	-1.52	-41.37
				recommended value:		-41.3
C <sub>2</sub> •C(OH)COOH + C <sub>2</sub> H <sub>6</sub> → C•C(OH)C + CCOOH	3.89	-43.37	1.24	-40.72	4.59	-44.07
C <sub>2</sub> •C(OH)COOH + C <sub>2</sub> H <sub>6</sub> → C <sub>2</sub> C(OH)C• + CCOOH	0.69	-44.36	-1.89	-41.79	-0.26	-43.42
				recommended value:		-43.7
C <sub>2</sub> C(OH)CHO + C <sub>2</sub> H <sub>6</sub> → C <sub>3</sub> CCHO + CH <sub>3</sub> OH	10.42	-97.00	8.63	-95.20	7.76	-94.33
C <sub>2</sub> C(OH)CHO + C <sub>3</sub> H <sub>8</sub> → C <sub>3</sub> CCHO + CCOH	6.57	-96.41	5.34	-95.18	4.81	-94.65
				recommended value:		-94.5

<sup>a</sup> Units in kcal mol<sup>-1</sup>.TABLE 2:  $\Delta H_f^\circ$  for Standard Species in Isodesmic Reactions

species	$\Delta H_f^\circ$ (kcal/mol)	ref
CH <sub>4</sub>	-17.89 ± 0.07	Cox et al <sup>21</sup>
C <sub>3</sub> CC	-40.14 ± 0.2	Good <sup>22</sup>
C <sub>2</sub> H <sub>6</sub>	-20.24 ± 0.12	Cox et al <sup>21</sup>
C <sub>2</sub> H <sub>5</sub>	28.80 ± 0.50	Marshall <sup>23</sup>
C <sub>3</sub> H <sub>8</sub>	-25.02 ± 0.12	Pedley et al <sup>24</sup>
CH <sub>3</sub> OH	-48.07 ± 0.05	Cox et al <sup>21</sup>
CCOH	-56.21 ± 0.10	Pedley et al <sup>24</sup>
CC•OH	-13.34 ± 0.84	Sun et al <sup>25</sup>
C•COH	-5.70 ± 0.85	Sun et al <sup>25</sup>
C•C(OH)C	-14.95 ± 2.8	Sun et al <sup>12</sup>
C <sub>3</sub> COH	-74.72 ± 0.21	Wiberg et al <sup>26</sup>
C <sub>3</sub> CO•	-23.14	Chen et al <sup>4</sup>
CH <sub>3</sub> OO•	-2.15 ± 1.22	Knyazev et al <sup>27</sup>
CCOOH	-39.7 ± 0.3	Chen et al <sup>28</sup>
C•COOH	10.96 ± 1.06	Chen et al <sup>28</sup>
CCOO•	-6.8 ± 2.3	Blanksby et al <sup>29</sup>
CCCOOH	-44.77 ± 0.41	Chen et al <sup>28</sup>
C <sub>3</sub> CCOO•	-27.61	Sun et al <sup>1</sup>
C <sub>3</sub> •CCOOH	-9.43	Sun et al <sup>1</sup>
C <sub>3</sub> CCHO	-58.74	Sun et al <sup>1</sup>
C <sub>2</sub> COOH	-49.0	Lay et al. <sup>30</sup>

and 1.38 Å. In the leaving C•H<sub>2</sub>OOH group, the O—O bond length increases to 1.46–1.48 Å.

The (C•H<sub>2</sub>OOH)\* radical formed in the reactions above is unstable, and it rapidly dissociates (exothermic) over a small barrier (0–4 kcal mol<sup>-1</sup>) to CH<sub>2</sub>O + OH.

**2. Thermochemical Properties:  $\Delta H_f^\circ$ ,  $S^\circ$ , and  $C_p$ (300) to  $C_p$ (1500).** Enthalpies of formation for reactants, intermediates, and products were calculated by isodesmic reaction analysis, total energy differences, or taken from available literature. The calculated reaction enthalpies and  $\Delta H_f^\circ$  values of reactants, peroxy adducts, and intermediates with isodesmic reactions are listed in Table 1. The  $\Delta H_f^\circ$  values of reference species used in isodesmic reaction analysis are listed in Table 2. The notation “C” in Tables 1 and 2 represents carbon with hydrogen atoms

assumed to fill the valence, and the notation “•” represents a radical site. For example, C<sub>2</sub>C•COH stands for 2-hydroxy-1,1-dimethylethyl radical, and C<sub>2</sub>C(OH)C• stands for 2-hydroxy-2-methylpropyl radical. These notations are kept in the text and data tables for simplicity. Furthermore, the notation “=” represents double bond, and “y” represents cyclic structure within the bracket.

The  $\Delta H_f^\circ$  for the saddle-point transition state structures were determined by incorporating the difference of the total energies between radical adducts and transition states and  $\Delta H_f^\circ$  of radical adducts. The enthalpies of 17 transition state structures in the isobutene—OH oxidation systems determined at the three different levels are listed in Table 3. The activation energies calculated at the B3LYP level agree with those at the CBSQ//B3LYP level for most isomerization (TS14, TS23, TS27), HO<sub>2</sub> concerted elimination (TS19, TS20),  $\beta$ -scission (TS18, TS24, TS25, TS26), and epoxide formation (TS28, TS29, TS30) reactions within ~2 kcal mol<sup>-1</sup>. The TS15 and TS16 are hydrogen-shift reactions to the peroxy oxygen from a carbon, and the DFT energies for TS15 and TS16 are higher than those of the CBS-Q energies by ~5 kcal mol<sup>-1</sup>. The B3LYP energies of TS17, TS22, TS26 for the  $\beta$ -scission reactions are 3–4 kcal mol<sup>-1</sup> lower compared to those of CBSQ//B3LYP. One isomerization reaction via TS27 was calculated at the CBS-QB3 level, and the activation energy was found to be 41.2 kcal mol<sup>-1</sup>, which is in good agreement with the 41.5 kcal mol<sup>-1</sup> determined from the CBSQ//B3LYP calculation. The enthalpies of formation for transition states calculated at the CBSQ//B3LYP level in Table 3 are considered reliable and were used in our kinetic analysis.

**Internal Rotor Analysis.** The internal rotational potentials versus dihedral angle on CH<sub>3</sub>—C, C—C, C—OH, C—OO•, and C—C• bonds were calculated at the B3LYP/6-31G(d,p) level. The potential curves for terminal methyl rotation (CH<sub>3</sub>—C) in C<sub>2</sub>C•COH, C<sub>2</sub>C(OH)C•, C<sub>2</sub>C(OH)COO•, and C<sub>2</sub>C(OO•)COH radicals exhibit the normal 3-fold symmetric barrier, with typical

**TABLE 3: Calculated Activation Energies at 298 K<sup>a</sup>**

transition state	B3LYP/ 6-31G(d,p)	B3LYP/ 6-311++G(3df,2p)	CBSQ// B3LYP
TS14 (HSO)	23.3	23.9	21.9
TS15 (HSC)	41.9	41.3	35.6
TS16 (HSC)	34.7	33.6	28.4
TS17 (BSC)	7.4	4.8	10.1 <sup>b</sup>
TS18 (BSC)	10.4	9.5	11.6
TS19 (HO <sub>2</sub> -CE)	35.2	33.1	31.9
TS20 (HO <sub>2</sub> -CE)	34.7	32.3	32.0
TS21 <sup>b</sup> (BSC)	22.1	17.9	14.9
TS22 (HSO)	16.8	17.4	22.8
TS23 (HSC)	28.1	26.3	26.7
TS24 <sup>b</sup> (BSC)	9.0	6.3	9.3
TS25 (BSC)	14.5	12.2	12.9
TS26 (BSC)	21.9	20.4	24.0
TS27 (HSC)	44.1	43.1	41.5
TS28 (EPF)	13.6	11.5	13.2
TS29 (EPF)	9.3	6.7	5.1
TS30 (EPF)	18.8	16.7	17.7

<sup>a</sup> Units in kcal mol<sup>-1</sup>, activation energies were calculated from forward reaction. Abbreviations: TS stands for transition state structure; HSO stands for H-shift from oxygen; HSC stands for H-shift from carbon; BSC stands for  $\beta$ -scission reaction; HO<sub>2</sub>-CE stands for HO<sub>2</sub> concerted elimination forming a sp<sup>2</sup> carbon structure. EPF stands for epoxide formation. <sup>b</sup> The activation energy was calculated based on the energy difference between transition state and peroxy adduct.

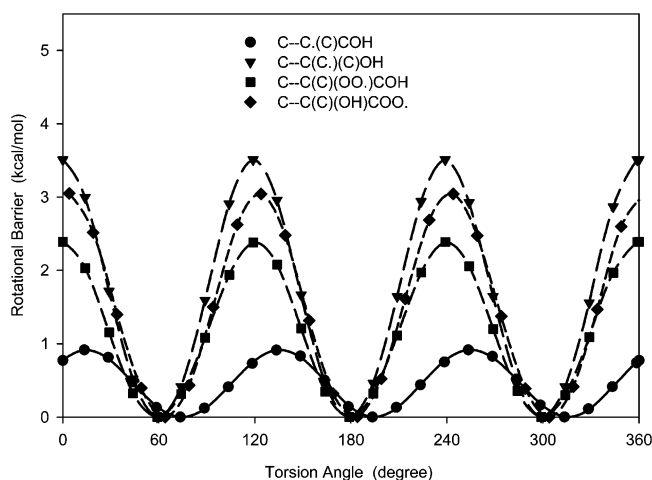


**Figure 1.** Internal rotation potentials on the CH<sub>3</sub>-C bond for C<sub>2</sub>C•COH, C<sub>2</sub>C(OH)C•, C<sub>2</sub>C(OH)COO•, and C<sub>2</sub>C(OO•)COH radicals calculated at B3LYP/6-31G(d,p) level.

values of 2.5–3.5 kcal mol<sup>-1</sup> as is in the normal C–C bond environment, see Figure 1. The barrier of the CH<sub>3</sub>-C rotor in the C<sub>2</sub>C•COH has lower value near 1 kcal mol<sup>-1</sup>, which is a result of reduced steric hindrance due to the methyl group being adjacent to a tertiary radical site.

Figure 2 shows the internal rotor on the C–C bonds in the C<sub>2</sub>C(OO•)–COH and C<sub>2</sub>C(OH)–COO• radicals, which have relatively high barriers, 4–9 kcal mol<sup>-1</sup>. These are 3-fold potentials, but each system has at least one barrier and one potential well that are unique.

The internal rotation potentials for the C–O and C–C• bonds are provided in the Supporting Information Figures S1–S3. The potential curves for internal rotors on the C–OH bond in C<sub>2</sub>C•C–OH, C<sub>2</sub>C(OH)C•, C<sub>2</sub>C(OH)COO•, and C<sub>2</sub>C(OO•)C–OH radicals are provided in Figure S1. The potentials in the two peroxy radicals C<sub>2</sub>C(OH)COO• and C<sub>2</sub>C(OO•)C–OH are complex, highly nonsymmetric, and show the different interactions of the –OH hydrogen through the rotation. These potentials range to about 6–7 kcal mol<sup>-1</sup>, which are higher than the 2.5–3 kcal mol<sup>-1</sup> for the nonperoxy radicals C<sub>2</sub>C•C–OH

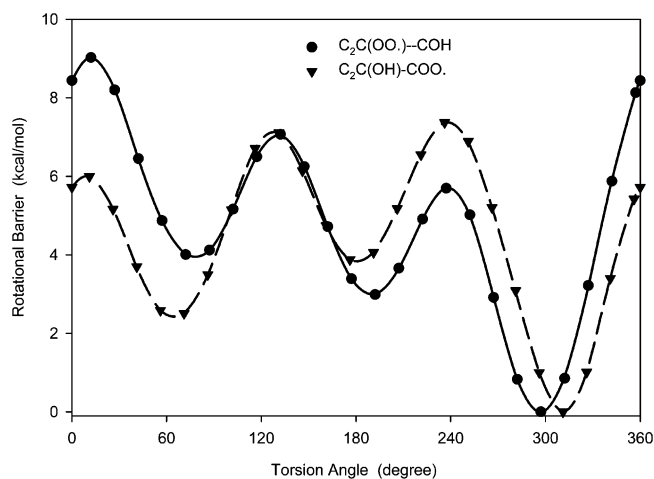


**Figure 2.** Internal rotation potentials on the C–C bond for C<sub>2</sub>C(OO•)–COH and C<sub>2</sub>C(OH)COO• radicals calculated at B3LYP/6-31G(d,p) level.

and C<sub>2</sub>C(OH)C•. Our further inspection on the higher barrier implies they are from the H atom on the –OH group interaction (hydrogen bonding) with the peroxyoxygen radical. Figure S2 illustrates the rotation potentials on the C–OO• bond in C<sub>2</sub>C(OH)COO• and C<sub>2</sub>C(OO•)COH radicals, where the barriers are 3–4 kcal mol<sup>-1</sup>; these are similar in complexity to the rotations of –OH groups. The rotation potentials on the C–C• bonds for the C<sub>2</sub>C•COH and C<sub>2</sub>C(OH)C• radicals have 2-fold barriers of 1.5–3.0 kcal mol<sup>-1</sup> as shown in Figure S3. The –CH<sub>2</sub> rotor has a barrier of 1.5 and is more symmetric than the C<sub>2</sub>C•–COH rotor, which has a 2-fold barrier with an average maximum of 2.6 kcal mol<sup>-1</sup>.

The potential barriers were used to calculate the contributions from internal rotors to entropy and heat capacities. Table 4 lists the contributions from vibration, translation, and external rotation as well as the contribution from each hindered internal rotor to S<sup>o</sup><sub>298</sub> and C<sub>p</sub>(T) for the C<sub>2</sub>C•COH, C<sub>2</sub>C(OH)C•, C<sub>2</sub>C(OO•)COH, and C<sub>2</sub>C(OH)COO• radicals. Table 5 lists the calculated thermochemical properties of reactants, transition states, intermediates, and products associated with the two reaction systems.

**3. Analysis of Chemical Activation Reactions. 3.1. C<sub>2</sub>C•COH + O<sub>2</sub> Reaction System.** A. Primary Reaction Paths of C<sub>2</sub>C•COH + O<sub>2</sub>. The potential energy diagram for the C<sub>2</sub>C•COH + O<sub>2</sub> reaction system calculated at the CBS-Q//B3LYP level is shown in Figure 3a,b. (The combined PE diagram, all paths, in Figure 3a,b are provided in Supporting Information Figure S4). The C<sub>2</sub>C•COH radical ( $\Delta H_f^{\circ}{}_{298} = -23.3$  kcal mol<sup>-1</sup>) reacts with O<sub>2</sub>(<sup>3</sup>Σ<sub>g</sub><sup>-</sup>) to form a chemically activated peroxy adduct C<sub>2</sub>C(OO•)COH\* with a 38.9 kcal mol<sup>-1</sup> well depth to the lowest energy adduct intermediate ( $\Delta H_f^{\circ}{}_{298} = -62.2$  kcal mol<sup>-1</sup>). This intermediate has the hydroxyl hydrogen in a hydrogen bonding with the peroxy radical. The energized peroxy adduct has sufficient energy to react over a number of isomerization and elimination barriers including three H atom shifts (isomerization) and two concerted HO<sub>2</sub> molecular elimination paths. In some cases, the isomer formed has more than sufficient energy to further dissociate to smaller and more stable products before its stabilization.

There are three isomerization (H-transfer) reaction paths for the C<sub>2</sub>C(OO•)COH adduct: (1) H atom transfer from the hydroxyl group to the peroxy radical site via a six-member ring TS14 ( $E_a = 21.9$  kcal mol<sup>-1</sup>) to form an alkoxy isomer C<sub>2</sub>C(OOH)CO•; (2) H atom transfer from a methyl group

TABLE 4: Calculated Contributions to Ideal Gas-Phase Thermodynamic Properties<sup>a</sup>

species	$\Delta H_f^\circ$ <sup>298</sup> <sup>b</sup>	$S^\circ$ <sub>298</sub> <sup>c</sup>	$C_p$ 300 <sup>c</sup>	$C_p$ 400	$C_p$ 500	$C_p$ 600	$C_p$ 800	$C_p$ 1000	$C_p$ 1500
C <sub>2</sub> C•COH (9) <sup>f</sup>	TVR <sup>d</sup>	67.77	18.67	24.57	30.22	35.17	43.07	48.99	58.29
	C–C•(C)COH <sup>e</sup>	5.48	1.42	1.26	1.18	1.13	1.07	1.04	1.02
	C–C•(C)COH <sup>e</sup>	5.48	1.42	1.26	1.18	1.13	1.07	1.04	1.02
	C <sub>2</sub> C•–COH <sup>e</sup>	6.42	2.41	2.19	1.96	1.77	1.50	1.34	1.15
	C <sub>2</sub> C•C–OH <sup>e</sup>	3.09	2.44	2.36	2.11	1.88	1.56	1.37	1.17
total	<b>–23.3</b>	<b>88.24</b>	<b>26.36</b>	<b>31.64</b>	<b>36.65</b>	<b>41.08</b>	<b>48.27</b>	<b>53.78</b>	<b>62.65</b>
C <sub>2</sub> C(OH)C• (9) <sup>f</sup>	TVR	67.85	20.78	26.83	32.24	36.84	44.09	49.57	58.39
	C <sub>2</sub> C(–OH)C• <sup>e</sup>	3.42	2.20	2.02	1.81	1.64	1.41	1.28	1.13
	C–C(C)(C•)COH <sup>e</sup>	4.26	2.07	2.14	2.08	1.97	1.73	1.54	1.28
	C–C(C)(C•)COH <sup>e</sup>	4.26	2.07	2.14	2.08	1.97	1.73	1.54	1.28
	C•–C(C <sub>2</sub> )OH <sup>e</sup>	4.61	1.75	1.55	1.41	1.31	1.19	1.13	1.06
total	<b>–24.2</b>	<b>84.40</b>	<b>28.87</b>	<b>34.68</b>	<b>39.62</b>	<b>43.73</b>	<b>50.15</b>	<b>55.06</b>	<b>63.14</b>
C <sub>2</sub> C(OO•)COH (9) <sup>f</sup>	TVR	73.15	23.48	30.62	37.13	42.69	51.34	57.67	67.50
	C <sub>2</sub> C(OO•)C–OH <sup>e</sup>	0.92	2.41	3.57	3.99	3.85	3.09	2.44	1.63
	C <sub>2</sub> C(OO•)–COH <sup>e</sup>	3.54	2.66	3.41	3.91	4.06	3.71	3.13	2.08
	C–C(C)(OO•)COH <sup>e</sup>	4.72	2.10	1.97	1.80	1.64	1.42	1.29	1.14
	C–C(C)(OO•)COH <sup>e</sup>	4.72	2.10	1.97	1.80	1.64	1.42	1.29	1.14
total	<b>–62.2</b>	<b>92.97</b>	<b>36.09</b>	<b>44.31</b>	<b>50.95</b>	<b>55.88</b>	<b>62.60</b>	<b>67.23</b>	<b>74.67</b>
C <sub>2</sub> C(OH)COO• (9) <sup>f</sup>	TVR	72.89	23.36	30.65	37.23	42.81	51.43	57.74	67.52
	C <sub>2</sub> C(OH)C–OO• <sup>e</sup>	5.54	4.04	3.33	2.68	2.23	1.72	1.46	1.19
	C <sub>2</sub> C(OO•)C–OH <sup>e</sup>	1.60	2.48	2.95	3.10	3.02	2.62	2.22	1.62
	C <sub>2</sub> C(OH)COO• <sup>e</sup>	5.58	2.95	3.25	3.29	3.14	2.6	2.07	1.21
	C–C(C)(OH)COO• <sup>e</sup>	4.38	2.15	2.16	2.04	1.89	1.63	1.45	1.22
total	<b>–61.8</b>	<b>94.37</b>	<b>37.13</b>	<b>44.50</b>	<b>50.38</b>	<b>54.98</b>	<b>61.63</b>	<b>66.39</b>	<b>73.98</b>

<sup>a</sup> Thermodynamic properties are referred to a standard state of an ideal gas at 1 atm. <sup>b</sup> Units in kcal mol<sup>–1</sup>. <sup>c</sup> Units in cal mol<sup>–1</sup> K<sup>–1</sup>. <sup>d</sup> The sum of contributions from translations, vibrations, and external rotations. <sup>e</sup> Contribution from internal rotations. <sup>f</sup> Symmetry number.

TABLE 5: Calculated Ideal Gas-Phase Thermodynamic Properties<sup>a</sup>

species	$\Delta H_f^\circ$ <sup>298</sup> <sup>b</sup>	$S^\circ$ <sub>298</sub> <sup>c</sup>	$C_p$ 300 <sup>c</sup>	$C_p$ 400	$C_p$ 500	$C_p$ 600	$C_p$ 800	$C_p$ 1000	$C_p$ 1500
C <sub>2</sub> C•COH	–23.3	88.24	26.36	31.64	36.65	41.08	48.27	53.78	62.65
C <sub>2</sub> C(OO•)COH	–62.2	92.97	36.09	44.31	50.95	55.88	62.60	67.23	74.67
C <sub>2</sub> •C(OOH)COH	–45.7	101.89	36.94	45.34	51.98	56.80	63.15	67.42	74.20
C <sub>2</sub> C(OOH)C•OH	–48.8	101.48	35.19	42.13	48.24	53.26	60.78	66.05	73.97
C <sub>2</sub> C(OOH)CO•	–43.5 <sup>d</sup>	98.39	34.53	42.22	48.83	54.11	61.71	66.95	74.82
C <sub>2</sub> C=COH	–49.5 <sup>e</sup>	80.02	25.98	31.14	35.75	39.73	46.12	51.01	58.89
C=C(C)COH	–39.8 <sup>f</sup>	83.04	24.68	29.78	34.45	38.49	44.97	49.91	57.83
C <sub>2</sub> C(OH)C•	–24.2	84.40	28.87	34.68	39.62	43.73	50.15	55.06	63.14
C <sub>2</sub> C(OH)COO•	–61.8	94.37	37.13	44.50	50.38	54.98	61.63	66.39	73.98
C <sub>2</sub> C(O•)COOH	–41.3	100.06	37.11	43.89	49.51	54.08	60.96	65.96	73.88
C <sub>2</sub> •C(OH)COOH	–43.7	102.52	39.35	46.35	51.85	56.06	62.08	66.39	73.40
CC(=O)COOH	–68.2 <sup>f</sup>	90.28	29.07	33.78	37.73	40.96	45.83	49.32	54.78
C <sub>2</sub> C(OH)CHO	–94.5	83.87	29.01	35.08	40.34	44.75	51.61	56.71	64.78
C <sub>γ</sub> (CCO)COH	–76.6	79.73	28.02	36.48	43.29	48.26	54.80	59.15	65.92
C <sub>2</sub> γ(COC)OH	–66.6	80.53	27.76	34.09	39.68	44.35	51.63	56.99	65.39
C <sub>γ</sub> (CCOC)OH	–71.3	76.99	24.06	31.02	37.18	42.30	50.08	55.69	64.30
TS14	–40.3	87.39	32.92	40.54	47.15	52.63	60.99	66.93	75.74
TS15	–26.7	86.50	33.45	43.06	50.63	56.14	63.35	68.09	75.34
TS16	–33.7	86.93	33.07	41.54	48.33	53.47	60.83	66.05	74.28
TS17	–33.4	94.83	34.31	40.64	46.34	51.23	59.02	64.87	74.12
TS18	–37.2	91.01	33.69	40.72	46.87	51.95	59.67	65.22	73.86
TS19	–30.2	90.56	34.09	41.98	48.48	53.50	60.80	66.04	74.30
TS20	–30.2	90.44	32.37	39.71	46.22	51.68	60.01	65.93	74.72
TS21	–30.8	91.76	33.73	40.86	46.97	52.02	59.82	65.58	74.75
TS22	–39.0	85.19	31.16	39.18	45.96	51.51	59.87	65.85	74.94
TS23	–35.0	85.38	31.78	40.02	46.94	52.54	60.86	66.76	75.74
TS24	–32.0	94.68	34.34	41.29	47.22	52.12	59.68	65.29	74.23
TS25	–28.4	97.46	38.14	44.72	50.05	54.36	60.87	65.70	73.53
TS26	–19.7	97.60	35.60	42.52	48.30	53.01	60.19	65.51	74.15
TS27	–20.6	91.86	33.60	40.98	47.20	52.29	59.96	65.50	74.10
TS28	–32.5	91.82	36.22	45.11	51.97	56.87	63.27	67.59	74.65
TS29	–43.7	92.71	35.29	41.98	47.66	52.36	59.67	65.13	73.98
TS30	–26.0	91.07	34.18	41.70	47.95	52.99	60.59	66.14	75.01

<sup>a</sup> Thermodynamic properties are referred to a standard state of an ideal gas at 1 atm. <sup>b</sup> Units in kcal mol<sup>–1</sup>. <sup>c</sup> Units in cal mol<sup>–1</sup> K<sup>–1</sup>. <sup>d</sup> Chen, C.-J., Bozzelli, J. W. *J. Phys. Chem. A* **1999**, *103*, 9731. <sup>e</sup> Turecek, F.; Brabec, L.; Korvola, J., *J. Am. Chem. Soc.* **1988**, *110*, 7984. <sup>f</sup> Bozzelli, Thermo Database.

via the five-member ring TS15 ( $E_a = 35.5$  kcal mol<sup>–1</sup>) to form an alkyl hydroperoxide C<sub>2</sub>•C(OOH)COH radical ( $\Delta H_f^\circ$ <sub>298</sub> = –45.7 kcal mol<sup>–1</sup>); (3) H atom transfer from the alcohol

carbon via the five-member ring TS16 ( $E_a = 28.4$  kcal mol<sup>–1</sup>) to form the radical C<sub>2</sub>C(OOH)C•OH ( $\Delta H_f^\circ$ <sub>298</sub> = –48.8 kcal mol<sup>–1</sup>).

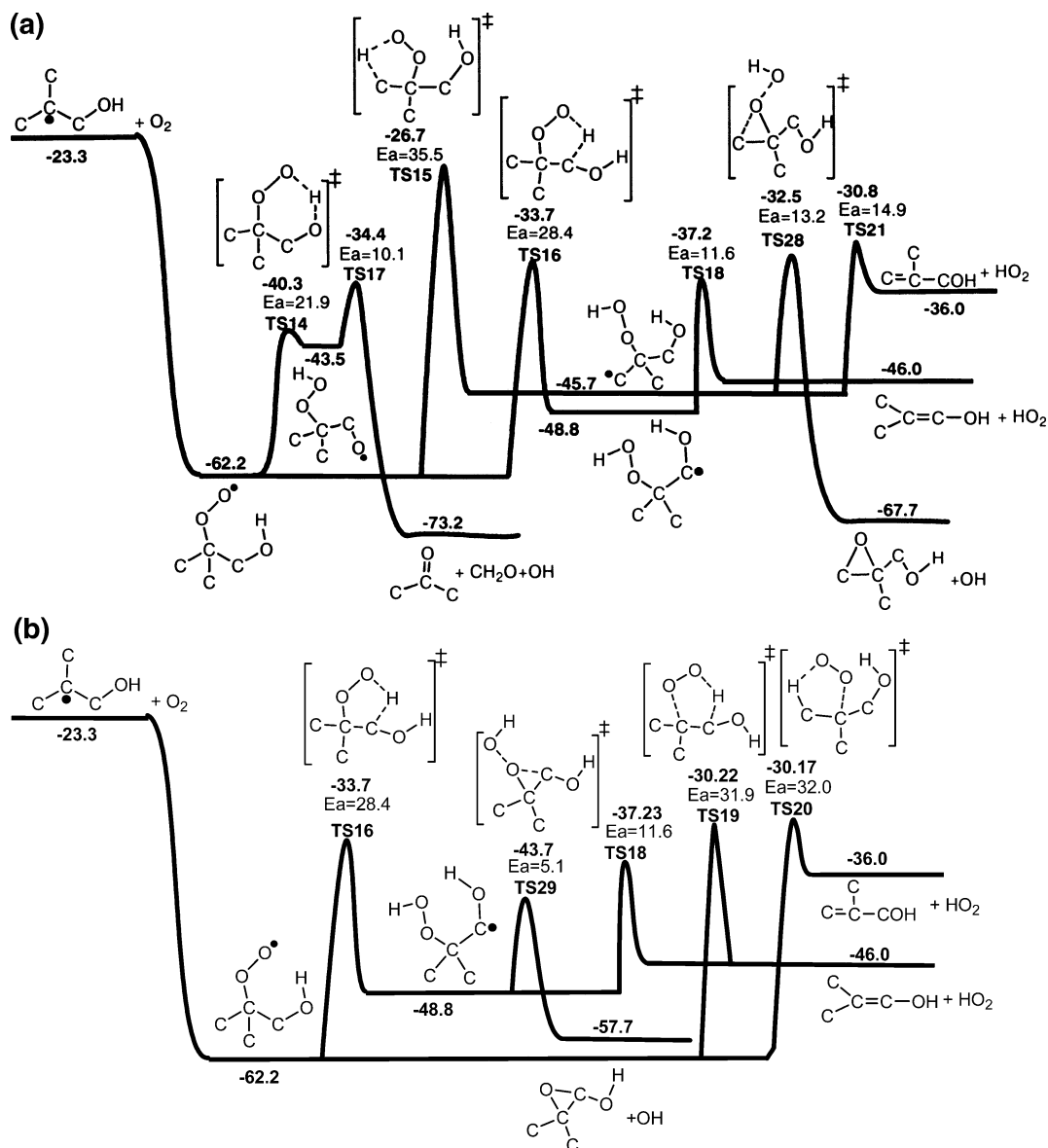


**Figure 3.** Potential energy diagram of  $C_2C\bullet COH + O_2$  reaction system calculated at the CBS-Q//B3LYP level. Unit in  $\text{kcal mol}^{-1}$ .

Two reaction paths for  $HO_2$  concerted elimination from the  $C_2C(OO\bullet)COH$  adduct were found as follows: (1) the peroxy oxygen interacts with the H atom on the alcohol carbon via the five-member ring TS19 ( $E_a = 31.9 \text{ kcal mol}^{-1}$ ) to form  $C=C(C)COH + HO_2$ ; (2) the peroxy oxygen attacks the H atom on the terminal methyl group, also via a five-member ring TS20 ( $E_a = 32.0 \text{ kcal mol}^{-1}$ ) to  $C_2C=COH + HO_2$  products.

**B. Reaction of Radical Intermediates: Hydroperoxide Alkyl and Alkoxy Radicals Formed via Isomerization(s) of the  $[C_2C(OO\bullet)COH]$  Peroxy Radical.** (1)  $\beta$ -Scission–Elimination Reactions. The alkoxy radical  $C_2C(OOH)CO\bullet$  ( $\Delta H_f^\circ_{298} = -43.5 \text{ kcal mol}^{-1}$ , formed via TS14), further dissociates to acetone +  $(C\bullet H_2OOH)^*$  via TS17 with a small ( $10 \text{ kcal mol}^{-1}$ ) barrier; the  $C\bullet H_2OOH$  radical immediately decomposes (exothermic) to formaldehyde + OH radical. The highest barrier in this two step reaction path is  $10 \text{ kcal mol}^{-1}$  below the energy of the activated peroxy adduct (reactants) formed initially. There is sufficient energy in the chemically activated peroxy radical for direct reaction via the Waddington mechanism<sup>31,32</sup> to the products of acetone, formaldehyde, and OH radical.

(2) Unsaturated (Olefin) Alcohol Formation. An illustrated above, one vinylic alcohol (2-methyl-1-propen-ol) and one non vinylic olefin alcohol may be formed via  $HO_2$  molecular

elimination from the peroxy radical formed initially. The hydroperoxide–alkyl radicals also form these two alcohols by  $\beta$ -scission ( $HO_2$  elimination) via reaction through TS18 and TS21 to form the  $C_2C=COH$  and  $C=C(C)COH$  alcohols plus  $HO_2$ , respectively.

(3) Epoxide Formation. The hydroperoxide–alkyl radicals also undergo intramolecular substitution via three-member ring transition states TS28 ( $E_a = 13.2 \text{ kcal mol}^{-1}$ ) and TS29 ( $E_a = 5.1 \text{ kcal mol}^{-1}$ ), resulting in two three-member ring epoxides + OH:  $Cy(CCO)COH$  ( $\Delta H_f^\circ_{298} = -76.6 \text{ kcal mol}^{-1}$ ) + OH,  $C_2y(CCO)OH$  ( $\Delta H_f^\circ_{298} = -66.6 \text{ kcal mol}^{-1}$ ) + OH.

**C. Kinetics of the  $C_2C\bullet COH + O_2$  Reaction System.** The calculated rate constants for the chemical activation product channels of this reaction:



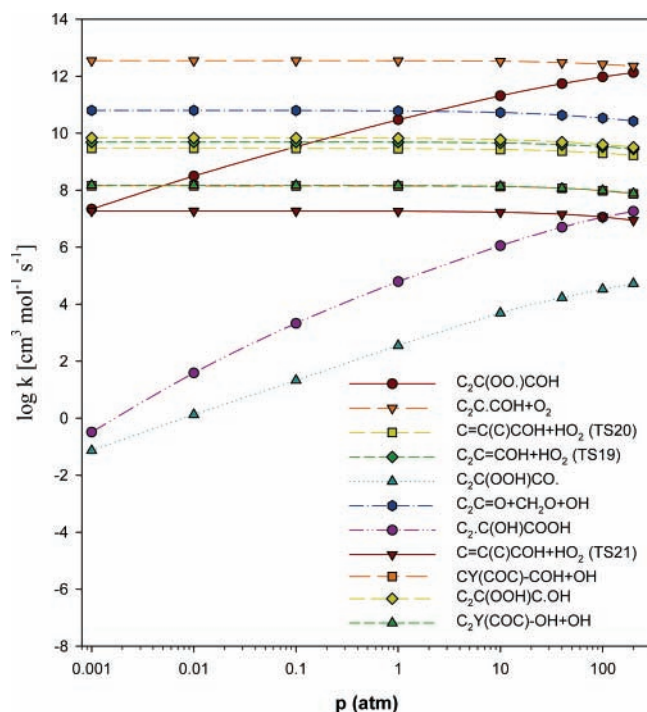
versus temperature at one atmosphere are illustrated in Figure 4, with the elementary rate parameters (high-pressure limit rate constants) listed in Table 6. The dominant product channel in this alkyl radical +  $O_2$  reaction system at 1 atm is stabilization to the  $C_2C(OO\bullet)COH$  peroxy radical below 700 K, and dissociation back to  $C_2C\bullet COH + O_2$  (nonreaction) is fast above



**TABLE 6: Elementary Rate Constants of the  $C_2C\bullet COH + O_2$  System**

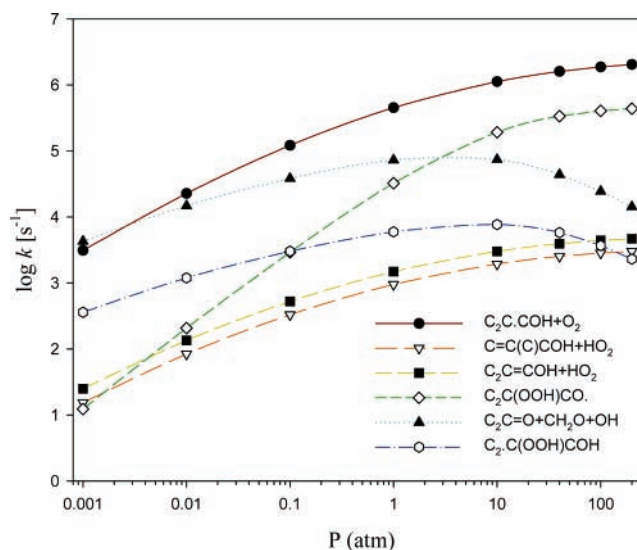
reaction <sup>c</sup>	elementary reaction rate constants		
	$A$ ( $s^{-1}$ or $cm^3 mol^{-1} s^{-1}$ )	$n$	$E_a$ ( $kal mol^{-1}$ )
$C_2C\bullet COH + O_2 \rightarrow C_2C(OO\bullet)COH$	$3.60 \times 10^{12a}$	0.0	0.0
$C_2C(OO\bullet)COH \rightarrow C_2C\bullet COH + O_2$	$1.39 \times 10^{16b}$	0.0	37.49
$C_2C(OO\bullet)COH \rightarrow C_2C(OOH)CO\bullet$	$2.91 \times 10^{12}$	-0.226	22.30
$C_2C(OO\bullet)COH \rightarrow C_2\bullet C(OOH)COH$	$2.52 \times 10^9$	0.780	35.34
$C_2C(OO\bullet)COH \rightarrow C_2C(OOH)C\bullet OH$	$3.97 \times 10^{12}$	-0.270	28.02
$C_2C(OO\bullet)COH \rightarrow C=C(C)COH + HO_2$	$3.64 \times 10^{14}$	-0.711	32.71
$C_2C(OO\bullet)COH \rightarrow C_2C=COH + HO_2$	$2.44 \times 10^{13}$	-0.253	32.59
$C_2C(OOH)CO\bullet \rightarrow C_2C(OO\bullet)COH$	$5.49 \times 10^8$	0.673	3.25
$C_2C(OOH)CO\bullet \rightarrow C_2C=O + CH_2O + OH$	$5.36 \times 10^{12}$	-0.080	10.79
$C_2\bullet C(OOH)COH \rightarrow C_2C(OO\bullet)COH$	$2.85 \times 10^8$	0.431	19.04
$C_2\bullet C(OOH)COH \rightarrow C_Y(CCO)COH + OH$	$1.58 \times 10^6$	1.613	12.60
$C_2\bullet C(OOH)COH \rightarrow C=C(C)COH + HO_2$	$6.12 \times 10^{13}$	-0.988	15.93
$C_2C(OOH)C\bullet OH \rightarrow C_2C(OO\bullet)COH$	$1.01 \times 10^7$	1.014	13.93
$C_2C(OOH)C\bullet OH \rightarrow C_2C=COH + HO_2$	$2.71 \times 10^9$	0.499	11.79
$C_2C(OOH)C\bullet OH \rightarrow C_2Y(CCO)OH + OH$	$3.19 \times 10^9$	0.634	5.38

<sup>a</sup> Atkinson, R.; Baulch, D. L.; Cox, R. A.; Hampson, R. F., Jr.; Kerr, J. A.; Troe, J. *J. Phys. Chem. Ref. Data* **1992**, *21*, 1125. <sup>b</sup> From the principle of microscopic reversibility, and  $E_a = H_{rxn}^\circ - RT$ . <sup>c</sup> Reduced frequency sets:  $C_2C(OO\bullet)COH$ : 250.2  $cm^{-1}$  (12.497), 1061.5  $cm^{-1}$  (20.396), 3470.9  $cm^{-1}$  (6.608).  $C_2C(OOH)CO\bullet$ : 339.1  $cm^{-1}$  (14.259), 1213.8  $cm^{-1}$  (18.651), 3448.4  $cm^{-1}$  (6.590).  $C_2\bullet C(OOH)COH$ : 250.0  $cm^{-1}$  (12.572), 1052.5  $cm^{-1}$  (20.962), 3582.5  $cm^{-1}$  (5.467).  $C_2C(OOH)C\bullet OH$ : 357.5  $cm^{-1}$  (15.906), 1324.6  $cm^{-1}$  (16.868), 3429.0  $cm^{-1}$  (6.227). Lennard-Jones parameters:  $\sigma = 5.86 \text{ \AA}$ ,  $\epsilon/k = 632 \text{ K}$ .

**Figure 5.** Calculated pressure dependence of rate constants for chemically activated  $C_2C\bullet COH + O_2$  system at  $T = 1000 \text{ K}$ .

which involves the more endothermic O—H bond transfer to the peroxy, is 3.9  $kal mol^{-1}$  lower than that of TS23. This lower barrier is a result of added energy in the adduct resulting from a prereaction complex with hydrogen-bonding between the hydroxyl hydrogen and the peroxy oxygen.

The H-shift from the peroxy radical carbon (ipso position, TS27) initially forms a substituted hydroperoxy—methyl radical, which rapidly dissociates via  $\beta$ -scission to form a strong carbonyl bond (aldehyde) while cleaving the weak RO—OH bond. The overall reaction is  $C_2C(OH)COO\bullet \rightarrow C_2C(OH)CHO + OH$  ( $\Delta H_f^\circ_{298} = -94.5 \text{ kcal mol}^{-1}$ ). This reaction proceeds through a four-member cyclic transition state structure forming the unstable intermediate  $[C_2C(OH)C\bullet OOH]^*$ , which rapidly

**Figure 6.** Calculated pressure dependence of rate constants for the dissociation of  $C_2C(OO\bullet)COH$  (stabilized) adduct at  $800 \text{ K}$ .

dissociates (exothermic, no barrier) to products  $C_2C(OH)CHO$  plus OH. This reaction channel is only important at temperatures above 1150 K due to the high barrier from strain in the four-member ring TS structure.

There are no  $HO_2$  molecular elimination paths in this  $C_2C(OH)COO\bullet$  system because there is no hydrogen atom on the carbon adjacent to the peroxy—carbon atom from which  $HO_2$  concerted elimination can occur.

**B. Reaction of Products from Isomerization of the  $[C_2C(OH)COO\bullet]$  Peroxy Radical.** (1)  $\beta$ -Scission of  $C_2C(O\bullet)COOH$  Radical. The alkoxy isomer  $C_2C(O\bullet)COOH$  formed by isomerization via TS22 undergoes  $\beta$ -scission over low barriers (9–13  $kal mol^{-1}$ ), decomposing to acetone +  $CH_2O$  + OH via TS24 and to  $CH_3 + CC(=O)COOH$  via TS25, respectively. The energized peroxy radical has sufficient energy to react directly to these product set channels (acetone +  $CH_2O$  + OH) and  $CH_3 + CC(=O)COOH$  before stabilization. The acetone product set is another reaction path, resulting in the Waddington mechanism products.

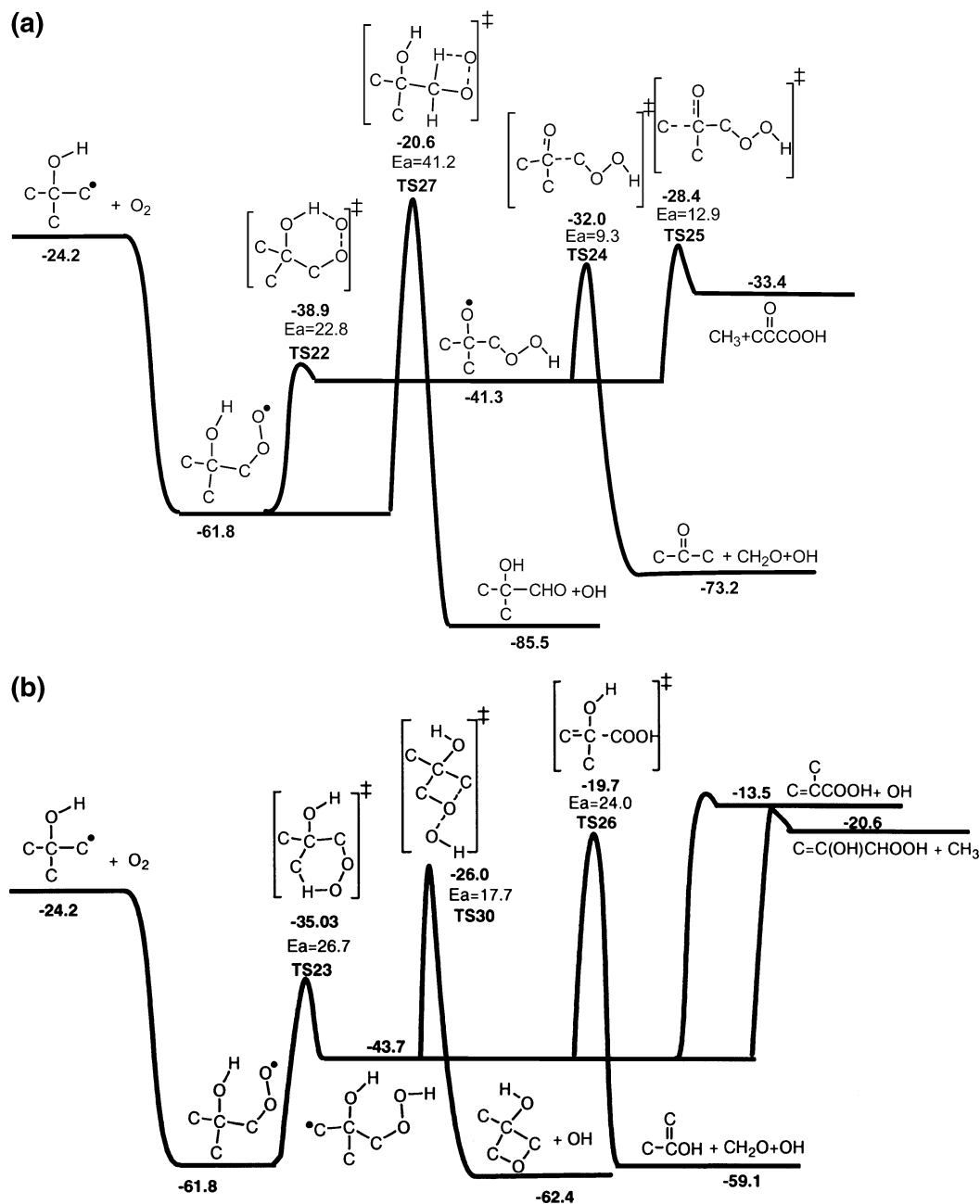


Figure 7. Potential energy diagram of  $\text{C}_2\text{C}(\text{OH})\text{C}^\bullet + \text{O}_2$  reaction system calculated at the CBS-Q//B3LYP level. Unit in kcal mol<sup>-1</sup>.

(2) Reaction of  $(\text{C}_2^\bullet\text{C}(\text{OH})\text{COOH})$  Radical. The hydroperoxide alkyl radical  $(\text{C}_2^\bullet\text{C}(\text{OH})\text{COOH})$  formed from TS23 can undergo unimolecular dissociation to form 2-hydroxy propene, (a vinylic alcohol)  $\text{C}=\text{C}(\text{OH})$ , plus  $\text{CH}_2\text{O}$  and  $\text{OH}$  by TS26, or 2-methylhydroperoxide propene ( $\text{C}=\text{C}(\text{C})\text{COOH}$ ) plus  $\text{OH}$ . The 2-methylhydroperoxide propene will undergo homolytic cleavage of the weak O—O bond in the peroxide moiety to generate an alkoxy radical ( $\text{C}=\text{C}(\text{C})\text{CO}^\bullet$ ) plus  $\text{OH}$  with a 42 kcal mol<sup>-1</sup> barrier. This alkoxy radical rapidly undergoes dissociation under combustion conditions to form a carbonyl and H atom ( $\text{C}=\text{C}(\text{C})\text{CO}^\bullet \rightarrow \text{C}=\text{C}(\text{C})\text{CH}=\text{O} + \text{H}$ ).

The hydroperoxide alkyl radical  $(\text{C}_2^\bullet\text{C}(\text{OH})\text{COOH})$  can also eliminate a methyl radical, forming a methyl—hydroperoxide—ethanol ( $\text{C}=\text{C}(\text{OH})\text{CH}_2\text{OOH}$ ). Similar to the methyl radical elimination from the hydroperoxide neopentyl radical,<sup>1</sup> this reaction is 20.6 kcal mol<sup>-1</sup> endothermic with

a 27 kcal mol<sup>-1</sup> barrier. This channel, as well as the product channel to  $\text{C}=\text{C}(\text{C})\text{COOH} + \text{OH}$ , are unimportant product channels because of the relatively high barriers and endothermicity.

The hydroperoxide alkyl radical  $(\text{C}_2^\bullet\text{C}(\text{OH})\text{COOH})$  can also undergo intramolecular substitution via TS30 ( $E_a = 17.7$  kcal mol<sup>-1</sup>) to form substituted oxitane products  $\text{C}(\text{OH})\text{y}(\text{CCOC})$  ( $\Delta H_f^\circ_{298} = -71.3$  kcal mol<sup>-1</sup>) +  $\text{OH}$ . In addition to the above reaction channels, the hydroperoxide alkyl radical  $(\text{C}_2^\bullet\text{C}(\text{OH})\text{COOH})$  can further react with molecular oxygen for chain branching reactions.<sup>34</sup>

C. Kinetics of the  $\text{C}_2\text{C}(\text{OH})\text{C}^\bullet + \text{O}_2$  Reaction System. The elementary unimolecular rate constants derived from the ab initio and density functional calculations and transition state theory for individual (elementary) reactions in this  $\text{C}_2\text{C}(\text{OH})\text{C}^\bullet + \text{O}_2$  reaction system are listed in Table 7. They are in the form of a three-parameter

TABLE 7: Elementary Rate Constants of the  $C_2C(OH)C\bullet + O_2$  System

reaction <sup>c</sup>	elementary reaction rate constants		
	$A$ ( $s^{-1}$ or $cm^3 mol^{-1} s^{-1}$ )	$n$	$E_a$ (kal $mol^{-1}$ )
$C_2C(OH)C\bullet + O_2 \rightarrow C_2C(OH)COO\bullet$	$3.60 \times 10^{12a}$	0.0	0.0
$C_2C(OH)COO\bullet \rightarrow C_2C(OH)C\bullet + O_2$	$2.66 \times 10^{15b}$	0.0	35.40
$C_2C(OH)COO\bullet \rightarrow C_2C(O\bullet)CQ$	$9.30 \times 10^{10}$	-0.036	22.89
$C_2C(OH)COO\bullet \rightarrow C_2\bullet C(OH)CQ$	$4.33 \times 10^9$	0.433	26.52
$C_2C(OH)COO\bullet \rightarrow C_2C(OH)CHO + OH$	$1.49 \times 10^9$	0.109	41.39
$C_2C(O\bullet)CQ \rightarrow C_2C(OH)COO\bullet$	$6.81 \times 10^8$	0.271	2.25
$C_2C(O\bullet)CQ \rightarrow C_2C=O + CH_2O + OH$	$7.04 \times 10^{10}$	0.363	9.46
$C_2C(O\bullet)CQ \rightarrow CH_3 + C(C=O)CQ$	$4.90 \times 10^9$	1.015	12.91
$C_2\bullet C(OH)CQ \rightarrow C_2C(OH)COO\bullet$	$3.25 \times 10^8$	0.159	8.45
$C_2\bullet C(OH)CQ \rightarrow C=C(C)OH + CH_2O + OH$	$5.38 \times 10^{11}$	0.070	24.80
$C_2\bullet C(OH)CQ \rightarrow C\gamma(CCOC)-OH + OH$	$7.06 \times 10^9$	0.184	17.21
$C_2\bullet C(OH)CQ \rightarrow C=C(C)COOH$	$5.29 \times 10^{13}$	-0.717	31.92

<sup>a</sup> Atkinson, R.; Baulch, D. L.; Cox, R. A.; Hampson, R. F., Jr.; Kerr, J. A.; Troe, J. *J. Phys. Chem. Ref. Data* **1992**, *21*, 1125. <sup>b</sup> From the principle of microscopic reversibility, and  $E_a = H_{rxn}^\circ - RT$ . <sup>c</sup> Reduced frequency sets:  $C_2C(OH)COO\bullet$ : 398.6  $cm^{-1}$  (18.221), 1277.8  $cm^{-1}$  (13.882), 3602.6  $cm^{-1}$  (7.397).  $C_2C(O\bullet)CQ$ : 390.3  $cm^{-1}$  (18.415), 1381.0  $cm^{-1}$  (13.909), 3559.6  $cm^{-1}$  (7.176).  $C_2\bullet C(OH)CQ$ : 362.0  $cm^{-1}$  (18.577), 1228.3  $cm^{-1}$  (13.149), 3672.4  $cm^{-1}$  (7.274). Lennard-Jones parameters:  $\sigma = 5.86 \text{ \AA}$ ,  $\epsilon/k = 632 \text{ K}$ .

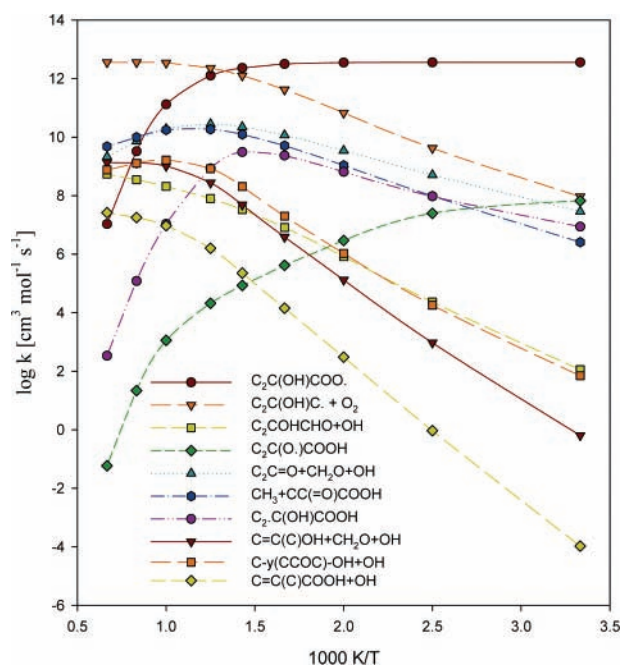


Figure 8. Calculated temperature-dependent rate constants for chemically activated  $C_2C(OH)C\bullet + O_2$  system at 1 atm.

Arrhenius fit,  $A_\infty$ ,  $n$ , and  $E_a$ , over the temperature range from 298 to 2000 K.



The calculated pressure-dependent rate constants for the chemical-activation reaction to products versus temperature at 1 atm are shown in Figure 8. The dominant product is stabilization to  $C_2C(OH)COO\bullet$  below 700 K. Dissociation of the chemically activated  $[C_2C(OH)COO\bullet]^*$  adduct (reaction back to  $C_2C(OH)C\bullet + O_2$ ) is also fast due to its loose transition state structure. This is a nonreaction and the reformed reactants can re-react. The most important product channels are the  $\beta$ -scissions of one isomerization adduct, a  $C_2C(O\bullet)COOH$  radical, to acetone +  $CH_2O$  + OH via TS24 and to  $CH_3 + CC(=O)COOH$  via TS25. The stabilization of another isomerization adduct,  $C_2\bullet C(OH)COOH$ , is important below 700 K but falls off rapidly above this temperature. The product sets of  $C_2C(OH)CHO + OH$  and methyl vinylic alcohol ( $C=C(C)OH$ ) plus  $CH_2O$  and OH start to become competitive with the ketone from the alkoxy isomer above 900 K.

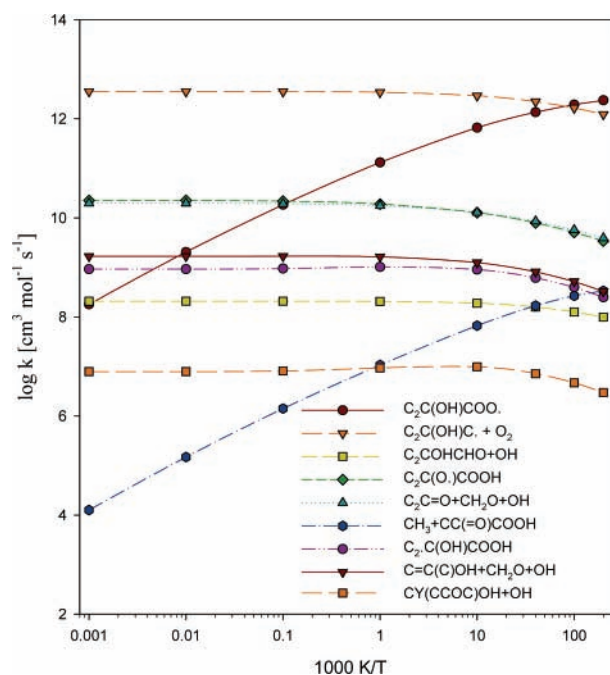
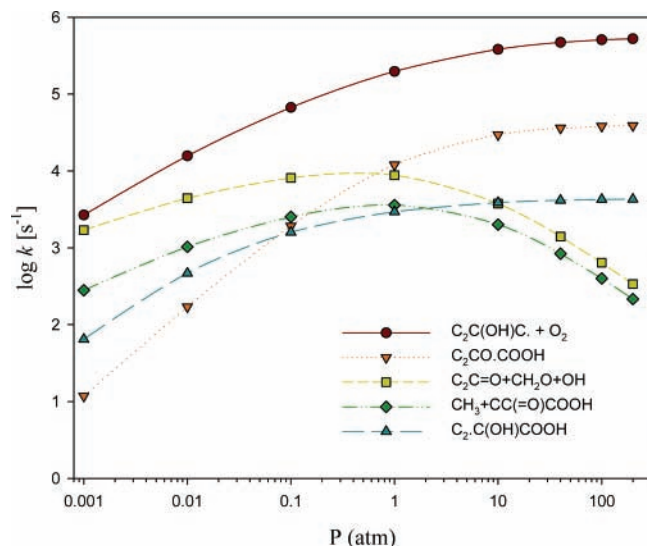


Figure 9. Calculated pressure dependence of rate constants for chemically activated  $C_2C(OH)C\bullet + O_2$  system at 1000 K.

The pressure-dependent rate constants of the important channels in this chemically activated  $C_2C(OH)C\bullet + O_2$  reaction, as determined from the QRRK and master equation analysis, are provided in Supporting Information Table S3 for pressures of 0.001, 0.01, 0.1, 1, 10, 40, 100, and 200 atm. The pressure-dependent rate constants for the dissociation of the stabilized adducts to products and to adjacent well isomers are also listed in Supporting Information Table S3.

The calculated pressure-dependent rate constants for the chemically activated  $C_2C(OH)C\bullet + O_2$  system at 1000 K are plotted in Figure 9. Stabilization of the chemically activated adduct  $C_2C(OH)COO\bullet$  has a strong pressure dependence at 1000 K. The product channel to  $CH_3 + CC(=O)COOH$  from the  $C_2C(O\bullet)COOH$  adduct also shows pressure dependence, but it is about 4 orders of magnitude below that of the peroxy radical stabilization. All other product channels exhibit falloff above 10 atm.

Figure 10 illustrates the pressure-dependent rate constants for the unimolecular dissociation of the stabilized  $C_2C(OH)COO\bullet$  peroxy adduct at 800 K. The important forward channels involve



**Figure 10.** Calculated pressure dependence of rate constants for the dissociation of  $C_2C(OH)COO\bullet$  adduct at 800 K.

the low barrier isomerization path to the  $C_2C(O\bullet)COOH$  adduct at higher pressures. The  $C_2C(O\bullet)COOH$  adduct will dissociate to  $CH_2O$  plus  $C_2C\bullet OOH$ , where the  $C_2C\bullet OOH$  will dissociate with no barrier to the lower energy products acetone plus OH. At lower pressures, the major products from dissociation of this  $C_2C(O\bullet)COOH$  adduct are acetone plus  $CH_2O + OH$ .

Our analyses on the chemical activation of these two isobutene–OH adducts with  $O_2(^3\Sigma_g^-)$  and the unimolecular dissociation of isobutene–OH– $O_2$  adducts indicate that: (1) the most important forward channel for the reaction system is the formation of acetone, formaldehyde, and OH, which is consistent with the Waddington mechanism;<sup>31,32</sup> (2)  $HO_2$  formation paths exist and contribute to the  $HO_2$  formation in the thermal oxidative reactions of neopentane. Furthermore, the OH radical, as shown by Taatjes et al.,<sup>2,3</sup> reacts with the neopentylperoxy radical ( $C_5H_{11}OO\bullet$ ) to form  $HO_2$  plus the neopentoxy radical  $C_5H_{11}O\bullet$ , which rapidly dissociates to *tert*-butyl radical and formaldehyde.

Isobutene and hydroxyl radical are important primary products from the  $O_2$  reaction with neopentyl radical,<sup>1,2</sup> and the OH is further formed by other reactions in the oxidative combustion of hydrocarbons. A further concern is that, at temperatures above 800 K, the unimolecular dissociation of neopentyl radical creates additional isobutene (plus methyl radical) and this process is in competition with that of neopentyl with  $O_2$  for loss of the neopentyl radical. The addition of OH to isobutene forms two important new radicals: 2-hydroxy-1,1-dimethylethyl and 2-hydroxy-2-methylpropyl radicals. The OH and  $HO_2$  product levels from the reaction of these hydroxyl–isobutane radicals with  $O_2$  may have strong effects on the respective concentration profiles.

One further reaction system that is needed as a submechanism for neopentyl oxidation is the methyl radical association with isobutene to form 2-methyl-2-butyl radical, (as opposed to reforming neopentyl radical). This 2-methyl-2-butyl radical can undergo association with  $O_2$  and further oxidation reactions. We identify this as the *isobutene–CH<sub>3</sub>–O<sub>2</sub> submechanism*. Our analysis on the chemical activation reaction of this 2-methyl-2-butyl (isobutene– $CH_3$  adduct) with  $O_2(^3\Sigma_g^-)$ , and the unimolecular dissociation of 2-methylbutane-2-peroxy radical, indicates that OH and  $HO_2$  radicals are important products from that system.<sup>35</sup> We incorporate the model results of the current study from the reactions of  $CH_3$  with isobutene and reactions

of the adducts with  $O_2$  in a separate manuscript that describes the thermochemistry and kinetics of the 2-methyl-2-butyl radical formation and its reactions with  $O_2$  and improved modeling of  $HO_2$  formation. Our extended reaction mechanism including the calculated isobutene–OH– $O_2$  and isobutene– $CH_3$ – $O_2$  submechanisms shows significant improvement for the modeling of  $HO_2$  formation in the neopentane oxidation.

## Summary

The stationary points on the potential energy surfaces of 2-hydroxy-1,1-dimethylethyl and 2-hydroxy-2-methylpropyl radicals with  $O_2(^3\Sigma_g^-)$  and the thermochemical properties of the species involved in these reaction systems were characterized based on ab initio and density functional theories. Internal rotation potential barriers for the reactants and intermediate peroxy adducts were also determined to accurately predict thermochemical properties for these oxy-generated species. The kinetic parameters for intermediate and product formation channels of the above systems were calculated as functions of temperature and pressure. High-pressure limit rate expressions for reaction channels on the potential energy surfaces are provided, and chemical activation and dissociation rate constants versus pressure and temperature are presented. These kinetic parameters can serve as models for branched alcohol oxidation mechanisms, where the radical site is adjacent to the alcohol carbon such as that in primary radical of ethanol and for other OH + olefin addition adducts.

The major products from the chemical activation reactions are those resulting from the Waddington mechanism, where an alkoxy radical is formed and subsequent  $\beta$ -scission reactions result in the formation of the strong  $\pi$  bonds of carbonyl products such as aldehydes and ketones. In addition, the reaction paths and kinetics of the hydroxyl–isobutene adducts with  $O_2(^3\Sigma_g^-)$  can also serve as models for similar  $\beta$ -hydroxy-ethyl radical reactions in ethanol combustion.

**Acknowledgment.** Partial Support by the Army Research Office, the Air Force Office of Scientific Research, and a Wright Patterson STTR Contract are gratefully acknowledged.

**Supporting Information Available:** Optimized geometries and structural parameters of 43 species including transition state structures are listed in Table S1. The corresponding unscaled vibrational frequencies and moments of inertia are listed in Table S2. Internal rotation potentials on the C–O and C–C• bonds are provided in Figures S1–S3. Combined potential energy diagrams for the  $C_2C\bullet COH + O_2$  and  $C_2C(OH)C\bullet + O_2$  reaction systems are provided in Figures S4–S5. Pressure-dependent rate constants on the reaction systems of  $C_2C\bullet COH + O_2$  and  $C_2C(OH)C\bullet + O_2$  are provided in Tables S3–S4.

## References and Notes

- (1) Sun, H.; Bozzelli, J. W. *J. Phys. Chem. A* **2004**, *108*, 1694.
- (2) DeSain, J. D.; Klippenstein, S. J.; Taatjes, C. A. *Phys. Chem. Chem. Phys.* **2003**, *5*, 1584.
- (3) Taatjes, C. A. *J. Phys. Chem. A* **2006**, *110*, 4299.
- (4) Chen, C.-J.; Bozzelli, J. W. *J. Phys. Chem. A* **1999**, *103*, 9731.
- (5) Ritter, E. R.; Bozzelli, J. W. *Int. J. Chem. Kinet.* **1991**, *23*, 767.
- (6) Stewart, J. J. P. *J. Comput. Chem.* **1989**, *10*, 2.
- (7) Stewart, J. J. P. *J. Comput. Chem.* **1989**, *10*, 10.
- (8) Lee, C.; Yang, W.; Parr, R. G. *Phys. Rev. B* **1988**, *37*, 785.
- (9) Frisch, M. J.; Trucks, G. W.; Schlegel, H. B.; Scuseria, G. E.; Robb, M. A.; Cheeseman, J. R.; Zakrzewski, V. G.; Montgomery, J. A., Jr.; Stratmann, R. E.; Burant, J. C.; Dapprich, S.; Millam, J. M.; Daniels, A. D.; Kudin, K. N.; Strain, M. C.; Farkas, O.; Tomasi, J.; Barone, V.; Cossi, M.; Cammi, R.; Mennucci, B.; Pomelli, C.; Adamo, C.; Clifford, S.; Ochterski, J.; Petersson, G. A.; Ayala, P. Y.; Cui, Q.; Morokuma, K.; Malick,

- D. K.; Rabuck, A. D.; Raghavachari, K.; Foresman, J. B.; Cioslowski, J.; Ortiz, J. V.; Stefanov, B. B.; Liu, G.; Liashenko, A.; Piskorz, P.; Komaromi, I.; Gomperts, R.; Martin, R. L.; Fox, D. J.; Keith, T.; Al-Laham, M. A.; Peng, C. Y.; Nanayakkara, A.; Gonzalez, C.; Challacombe, M.; Gill, P. M. W.; Johnson, B. G.; Chen, W.; Wong, M. W.; Andres, J. L.; Head-Gordon, M.; Replogle, E. S.; Pople, J. A. *Gaussian 98*, revision A.9; Gaussian, Inc.: Pittsburgh, PA, 1998.
- (10) Frisch, M. J.; Trucks, G. W.; Schlegel, H. B.; Scuseria, G. E.; Robb, M. A.; Cheeseman, J. R.; Montgomery, J. A., Jr.; Vreven, T.; Kudin, K. N.; Burant, J. C.; Millam, J. M.; Iyengar, S. S.; Tomasi, J.; Barone, V.; Mennucci, B.; Cossi, M.; Scalmani, G.; Rega, N.; Petersson, G. A.; Nakatsuji, H.; Hada, M.; Ehara, M.; Toyota, K.; Fukuda, R.; Hasegawa, J.; Ishida, M.; Nakajima, T.; Honda, Y.; Kitao, O.; Nakai, H.; Klene, M.; Li, X.; Knox, J. E.; Hratchian, H. P.; Cross, J. B.; Bakken, V.; Adamo, C.; Jaramillo, J.; Gomperts, R.; Stratmann, R. E.; Yazyev, O.; Austin, A. J.; Cammi, R.; Pomelli, C.; Ochterski, J. W.; Ayala, P. Y.; Morokuma, K.; Voth, G. A.; Salvador, P.; Dannenberg, J. J.; Zakrzewski, V. G.; Dapprich, S.; Daniels, A. D.; Strain, M. C.; Farkas, O.; Malick, D. K.; Rabuck, A. D.; Raghavachari, K.; Foresman, J. B.; Ortiz, J. V.; Cui, Q.; Baboul, A. G.; Clifford, S.; Cioslowski, J.; Stefanov, B. B.; Liu, G.; Liashenko, A.; Piskorz, P.; Komaromi, I.; Martin, R. L.; Fox, D. J.; Keith, T.; Al-Laham, M. A.; Peng, C. Y.; Nanayakkara, A.; Challacombe, M.; Gill, P. M. W.; Johnson, B.; Chen, W.; Wong, M. W.; Gonzalez, C.; Pople, J. A. *Gaussian 03*, revision B.04; Gaussian, Inc.: Pittsburgh PA, 2003.
- (11) Ochterski, J. W.; Petersson, G. A.; Montgomery, J. A. *J. Chem. Phys.* **1996**, *104*, 2598.
- (12) Sun, H.; Bozzelli, J. W. *J. Phys. Chem. A* **2002**, *106*, 3947.
- (13) Chen, C.-C.; Bozzelli, J. W.; Farrell, J. T. *J. Phys. Chem. A* **2004**, *108*, 4632.
- (14) Lay, T. H.; Krasnoperov, L. N.; Venanzi, C. A.; Bozzelli, J. W.; Shokhirev, N. V. *J. Phys. Chem.* **1996**, *100*, 8240.
- (15) Shokhirev, N. V. *Quantum Rotator*; <http://www.chem.arizona.edu/faculty/walk/nikolai/programs.html#rotor>, 1999.
- (16) Chang, A. Y.; Bozzelli, J. W.; Dean, A. M. *Z. Phys. Chem.* **2000**, *214*, 1533.
- (17) Sheng, C. Y.; Bozzelli, J. W.; Dean, A. M.; Chang, A. Y. *J. Phys. Chem. A* **2002**, *106*, 7276.
- (18) Bozzelli, J. W.; Chang, A. Y.; Dean, A. M. *Int. J. Chem. Kinet.* **1997**, *29*, 161.
- (19) Ben-Amotz, D. H.; Dudley, R. *J. Phys. Chem.* **1990**, *94*, 1038.
- (20) Somayajulu, G. R. *J. Chem. Eng. Data* **1989**, *34*, 106.
- (21) Cox, J. D.; Pilcher, G. *Thermochemistry of Organic & Organometallic Compounds*; Academic Press: New York, 1970.
- (22) Good, W. D. *J. Chem. Thermodyn.* **1970**, *2*, 237.
- (23) Marshall, P. *J. Phys. Chem. A* **1999**, *103*, 4560.
- (24) Pedley, J. B.; Naylor, R. D.; Kirby, S. P. *Thermochemical Data of Organic Compounds*, 2nd ed.; Chapman and Hall: New York, 1986.
- (25) Sun, H.; Bozzelli, J. W. *J. Phys. Chem. A* **2001**, *105*, 9543.
- (26) Wiberg, K. B.; Hao, S. *J. Org. Chem.* **1991**, *56*, 5108.
- (27) Knyazev, V. D.; Slage, I. R. *J. Phys. Chem.* **1998**, *102*, 1770.
- (28) Chen, C.-J.; Bozzelli, J. W. *J. Phys. Chem. A* **2000**, *104*, 4997.
- (29) Blanksby, S. J.; Ramond, T. M.; Davico, G. E.; Nimlos, M. R.; Kato, S.; Bierbaum, V. M.; Lineberger, W. C.; Ellison, G. B.; Okumura, M. *J. Am. Chem. Soc.* **2001**, *123*, 9585.
- (30) Lay, T. H.; Bozzelli, J. W. *J. Phys. Chem. A* **1997**, *101*, 9505.
- (31) Ray, D. J. M.; Waddington, D. J. *Combust. Flame* **1973**, *20*, 327.
- (32) Sway, M. I.; Waddington, D. J. *J. Chem. Soc., Perkin Trans.* **1983**, *2*, 139.
- (33) Taatjes, C. A.; Hansen, N.; McIlroy, A.; Miller, J. A.; Senosiain, J. P.; Klippenstein, S. J.; Qi, F.; Sheng, L.; Zhang, Y.; Cool, T. A.; Wang, J.; Westmoreland, P. R.; Law, M. E.; Kasper, T.; Kohse-Hoeinghaus, K. *Science* **2005**, *308*, 1887.
- (34) Bozzelli, J. W.; Sheng, C. *J. Phys. Chem. A* **2002**, *106*, 1113.
- (35) Sun, H.; Bozzelli, J. W.; Law, C. K. Thermochemical and Kinetic Analysis on Tertiary Alkyl Radicals with Oxygen: 2-Hydroxy-1, 1-Dimethylethyl and 1,1-Dimethylpropyl Radicals, *37th ACS Middle Atlantic Regional Meeting*, Rutgers University, New Brunswick, NJ, 2005.